Microporous and Mesoporous Materials 181 (2013) 254–261

Contents lists available at ScienceDirect

Microporous and Mesoporous Materials

journal homepage: www.elsevier.com/locate/micromeso

The influence of process conditions and Ostwald ripening on the specific surface area of olivine nano-silica

A. Lazaro [a,*], M.C. van de Griend [a], H.J.H. Brouwers [a], J.W. Geus [b]

[a] Department of the Built Environment, Eindhoven University of Technology, P.O. Box 513, 5600 MB Eindhoven, The Netherlands
[b] Debye Institute for Nanomaterials Science, University of Utrecht, Utrecht, The Netherlands

ARTICLE INFO

Article history:
Received 14 June 2013
Received in revised form 19 July 2013
Accepted 8 August 2013
Available online 17 August 2013

Keywords:
Olivine
Nano-silica
Specific surface area
Ostwald ripening
Porous material

ABSTRACT

The production of porous amorphous nano-silica by the olivine route is an interesting alternative to the existing commercial production methods because of the much lower energy requirements of this process. The produced olivine nano-silica has a specific surface area between 100 and 400 m^2/g and primary particles between 10 and 25 nm (agglomerated in clusters). The process conditions of the dissolution of olivine and the subsequent ripening treatment influence the specific surface area of the nano-silica in the following ways. (1) The cleaner the nano-silica is, the higher the specific surface area is. Thus, high-purity silicas presents an SSA between 300 and 400 m^2/g. (2) The higher the filtration pressure is, the higher the surface area will be. (3) The ripening treatment can diminish the specific surface of nano-silica by three quarters and reduce the microporous surface area by 90%. A 99% pure nano-silica with specific surface area controlled between 90 and 400 m^2/g can be synthesized by ripening treatment in an alkaline solution at room temperature. Therefore, tailored olivine nano-silica can provide additional environmental and economic benefits over the current commercial products.

1. Introduction

Nanotechnology and nanomaterials have attracted a great deal of attention in the previous years as can be seen from the fact that the number of patents has increased by 600% from 1992 to 2002 [1] and the annual global turnover is estimated to increase up to € 1.5 trillion by 2015 [2]. Nano-silica is one of the compounds that is boosting the field of nanomaterials with an annual rise of 6.3% reaching 2.7 million metric tons in 2014 and with a total value of $5.8 billion [3]. Nowadays, the two most important commercial processes in the production of nano-silica are the neutralization of sodium silicate solutions (commonly known as waterglass) with acid and the flame hydrolysis of silicon tetrachloride. Both processes are expensive and not environmentally friendly because of the high temperature steps, usually above 1000 °C, involved in these processes. In our previous work [4], it was stated that the production of nano-silica by the dissolution of olivine is an interesting alternative to the commercial methods because of the good quality of the resulting silica, and the low temperatures required (50–90 °C), which makes it cheaper and more sustainable.

The specific surface area (SSA) is a crucial parameter for nanomaterials conferring upon them special properties. This is because materials with a huge surface area possess a huge surface energy, and, thus, they are thermodynamically unstable or metastable [5]. Therefore, the application of these materials strongly depends on this parameter making it one of the most relevant parameters to study in the field of nano-materials. Olivine nano-silica is agglomerated in clusters forming a porous 3-D network structure with a high SSA. The agglomerated state of this silica can be beneficial for some applications where high-porous agglomerates are needed, such as nano-silica for ink-jet paper or catalytic materials. However, no research has been carried out regarding how to tailor the SSA of olivine nano-silica in order to fit the requirements of different applications.

The main purpose of this research is to establish the influence of the process conditions and the ripening treatment on the SSA of olivine nano-silica in order to assess the possibility of having a method to tailor olivine nano-silica. The results shown hear demonstrate that olivine nano-silica (with purity above 99%) in the range of 90–400 m^2/g can be produced using an Ostwald ripening treatment of the olivine nano-silica at 20 °C. Therefore, tailored olivine nano-silica can be produced for different applications, with the environmental and economic benefits that the use of this new nano-silica represents.

1.1. Olivine nano-silica process

The dissolution of olivine in acid at low temperatures produces amorphous silica:

* Corresponding author. Tel.: +31 (0)40 247 3411.
E-mail address: a.lazaro.garcia@tue.nl (A. Lazaro).

1387-1811/$ - see front matter © 2013 Elsevier Inc. All rights reserved.
http://dx.doi.org/10.1016/j.micromeso.2013.08.006

$$(Mg, Fe)_2SiO_4 + 4H^+ \rightarrow Si(OH)_4 + 2(Mg, Fe)^{2+}$$

The dissolution yields a slurry consisting of a mixture of magnesium/iron salts, silica, unreacted olivine and inert minerals (see Fig. 1). Once the reaction is complete, the unreacted olivine and inert minerals are removed from the final suspension by sedimentation. Subsequently, the silica can be cleaned from the resulting mixture by washing and filtering. After the filtration, a cake with around 20% solid content of nano-silica is obtained.

In our previous work, an olivine nano-silica with an SSA between 100 and 300 m^2/g, primary particles between 10 and 25 nm and purities above 95% was reported (see Table 1) [4]. The primary particles were agglomerated in clusters (see Fig. 2) forming a porous material with an average pore diameter above 10 nm. In addition, it was stated that the SSA of olivine nano-silica depends on the kinetics of the reaction of olivine and the amount of magnesium sulfate remaining in the material. In the current article we focus on the following points: (1) washing steps required to obtain purities above 99%; (2) influence of the sulfates on the SSA (SSA_{BET}, SSA_{MP} and SSA_E); (3) influence of the filtration pressure on the SSA; and (4) influence of post treatments, such as the Ostwald ripening, on the SSA.

1.2. Ostwald ripening theory

The Ostwald ripening consists of a hydrothermal treatment at basic pH in order to modify the equilibrium of the solubility of silica. The solubility equilibrium is reached when the rate of solution is equal to the rate of the deposition/condensation. The solubility of silica depends on the solution pH, the temperature, the radius of curvature of the silica particles and the content of impurities. In our particular case, the impurity content is not as relevant due to the low content of magnesium and iron ions and the inability of sulfate ions to alter the solubility of the silica [6]. Regarding the pH and temperature, the solubility of silica increases when these parameters rise [6]. In addition, the solubility of silica is higher for convex surfaces than for concave surfaces, and the radius of curvature has two main consequences for the solubility: the first consequence is that in a dispersion with individual particles of two sizes, the smaller particles dissolve faster than the larger ones. The second consequence is that in a dispersion with agglomerated particles and individual particles, the individual particles dissolve faster than the agglomerates, and the deposition of silica proceeds most rapidly at the point of contact between particles in the agglomerates due to the negative radius of curvature. These two consequences are graphically described in Figs. 3 and 4. Thus, when a silica dispersion is not in equilibrium, the more soluble particles dissolve. Subsequently, the soluble silica condensates on the surface of silica particles of lower solubility. The solution/deposition process will continue until a new equilibrium is reached. Another important factor in the solubility equilibrium of silica is the particle size distribution. This can be easily illustrated with the following example: a monomodal narrow particle size distribution would not be affected by a change in pH from 4 to 11 because, although the solubility of silica is much higher at pH 11 than at pH 4 [6], when the size of all the particles is the same, the ripening stops.

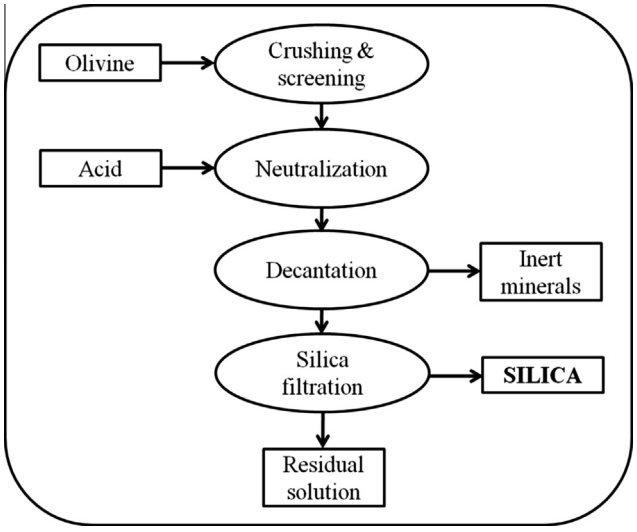

Fig. 1. Schematic process flow diagram of the olivine nano-silica process.

Table 1
Summary of the properties of different amorphous nano-silicas.

Parameters	Pyrogenic	Precipitated	Olivine route
Purity, SiO_2 (%)	>99.8	>95	>95
SSA_{BET} (m^2/g)	50–400	30–500	100–400
d (nm)	5–50	5–100	10–25
d_p (nm)	None	>30	20
Reference	[19]	[19]	[4]

Where d is particle size and d_p is pore diameter.
Table presented in [4].

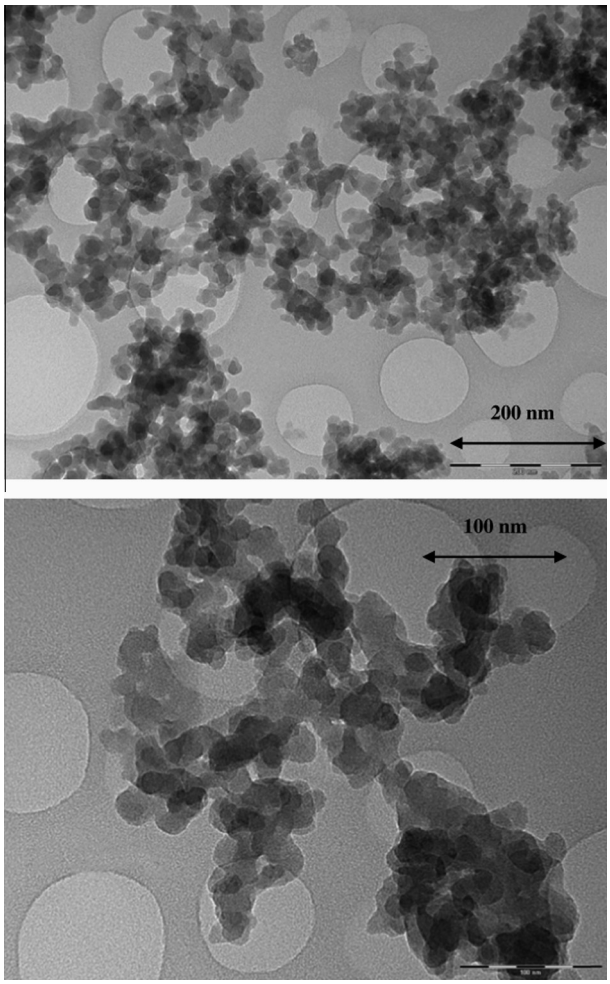

Fig. 2. Transmission electron microscope photographs (89 kx and 175 kx, respectively) of nano-silica produced by the dissolution of olivine.

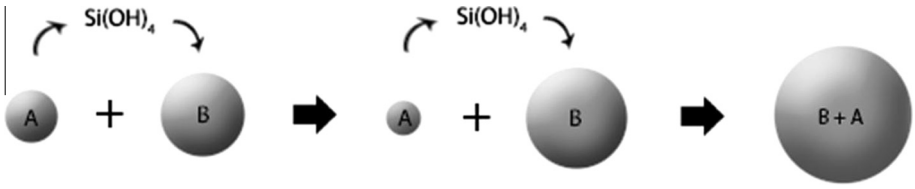

Fig. 3. Ostwald ripening representation when two individual particles of different sizes are present in a dispersion.

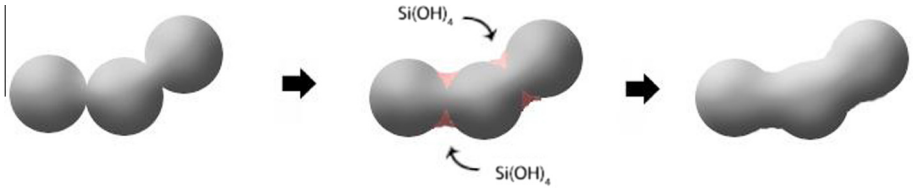

Fig. 4. Ostwald ripening representation when agglomerates are present in a dispersion.

2. Experimental method

The nano-silica synthesis experiments were carried out in a stirred glass thermostated reactor of one liter. The reagents used were 500 ml of 3 M sulfuric acid and a stoichiometric amount of olivine, previously dried. The ground olivine had a purity content of 89 wt.% of olivine with the composition $(Mg_{1.84}Fe_{0.153}Ni_{0.007})SiO_4$. The neutralization reaction was stopped when the concentration of $[H^+]$ reached 0.1 mol/l. Then, the solution was separated from the solid residue by sedimentation. Subsequently, the slurry was washed and filtered either using a vacuum pump (P_{abs} = 0.2 bar) or a filter press (P_{abs} = 3–5 bar).

The ripening experiments were performed in a stirred glass thermostated reactor of two liters with an olivine nano-silica supplied by Geochem. This material was supplied in a cake form with a solid content around 20 wt.%. The Ostwald ripening treatment was carried out in an alkaline solution using either NH_4OH or NaOH. The pH was adjusted to the desired value and kept constant during the experiments. Experiments were carried out at 20 °C and 90 °C, in the pH range between 4.6 and 11, and with a silica content between 3 and 6 wt.%. A high shear mixer (Silverson multifunctional L5M laboratory mixer with a shear screen) and an ultrasound bath (Powersonic 1100d with an effective power of 200 W) were used in some of the experiments. During the ripening process, samples were taken at regular intervals to determine the pH of the solution and the SSA of the dried silica. The silica samples were filtered and dried in an oven at 110 °C for about 15 h.

The nano-silica produced was characterized by nitrogen physisorption, transmission electron microscopy (TEM), X-ray fluorescence (XRF), combustion infrared analysis (determination of sulfur content) and laser light scattering (LLS). The XRF and the infrared analyses were carried out in Canada by Actlab laboratories using routines 4C and 4F, respectively. The LLS analyses were performed using a Mastersizer 2000. A Micromeritics TriStar 3000 equipment using N_2 and with a soaking time of 240 min at 190 °C was used for the gas physisorption analysis [7]. The physisorption analyses were performed three times with a standard deviation below 5%. The specific surface area (SSA_{BET}), the specific micropore surface area (SSA_{MP}), the specific external surface area (SSA_E) and the pore size distribution were calculated using the BET [7,8], t-plot [9,10] and BJH methods [11], respectively. The SSA_E was determined with the slope of the t-plot [12]. The particle size of the nano-silica was calculated from the geometrical relationship between surface area and mass given by

$$d\ (nm) = \frac{6000}{SSA_{BET} \cdot \rho} \quad (1)$$

where d is the particle size of nano-silica considered to be spherical (nm), ρ the density of the material (2.2 g/cm^3 for nano-silica) and SSA the surface area (m^2/g). This particle size is an average value considering that the particles are spherical. The micropore volume (V_{MP}) and the pore volume between 1.7 and 300 nm (V_P) were calculated using the BJH method [11].

3. Results

3.1. Influence of the process conditions

The olivine silicas were synthesized using several process conditions. The process conditions studied were the number of washing steps using a vacuum pump and the filtration pressure during the washing. Table 2 shows the SSA, the increase in the SSA between samples with consecutive filtration steps, the particle size (calculated using Eq. (2)), and the average pore size in the adsorption branch of the silicas; this table also shows the micropore volume and the pore volume in the adsorption branch. Table 3 presents the chemical composition, the purity of silica, the

Table 2
SSA, increase in the SSA between samples with consecutive filtration steps, particle size, pore size in the adsorption branch, micropore volume and pore volume in the adsorption branch.

Sample	SSA_{BET} (m^2/g)	SSA_{MP} (m^2/g)	SSA_E (m^2/g)	ΔSSA_{BET} (%)	ΔSSA_{MP} (%)	ΔSSA_E (%)	d (nm)	d_{p_A} (nm)	V_{MP} (cm^3/g)	V_{P_A} (cm^3/g)
NS-3F	233	58	175	–	–	–	11.7	14.5	0.025	0.529
NS-4F	324	122	202	39	110	15	8.4	13.9	0.055	0.578
NS-5F	346	142	204	7	16	1	7.9	13.7	0.064	0.589
NS-6F	348	142	206	0	0	1	7.8	14.6	0.064	0.679
NS-HP	433	125	308	–	–	–	6.3	14.7	0.055	1.026

F refers to washing/filtration steps and HP to high pressure filtration.

Table 3
Chemical composition, purity and conductivity of the olivine nano-silicas with different number of filtration steps, of a filter-pressed olivine nano-silica, and of the raw material used in the Ostwald ripening experiments.

Sample	SiO_2 (%)	Al_2O_3 (%)	Fe_2O_3 (%)	MgO (%)	CaO (%)	K_2O (%)	Cr_2O_3 (%)	LOI (%)	S (%)	Psi (%)	Cond. (mS)	m_{T_im} (%)
NS-3F	86.05	0.02	0.21	1.35	0.01	0.01	0.02	12.33	1.75	93.96	52.60	6.654
NS-4F	91.64	0.09	0.07	0.38	0.01	0.01	0.02	7.77	0.33	98.59	12.30	1.402
NS-5F	92.56	0.12	0.05	0.21	0.01	0.01	0.02	7.01	0.05	99.45	2.47	0.216
NS-6F	92.42	0.30	0.04	0.22	0.05	0.03	0.02	6.92	0.03	99.27	0.32	0.129
NS-HP	85.70	0.02	1.00	1.66	0.04	0.01	0.03	11.54	1.26	94.07	0.33	–
RM	90.29	0.05	0.21	0.26	0.03	0.03	0.02	9.10	0.06	99.24	–	–

P_{Si} was calculated using Eq. (3).
F refers to washing/filtration steps, HP high pressure filtration and RM raw materials.
In the Appendix, calculation of m_{T_im} is shown.

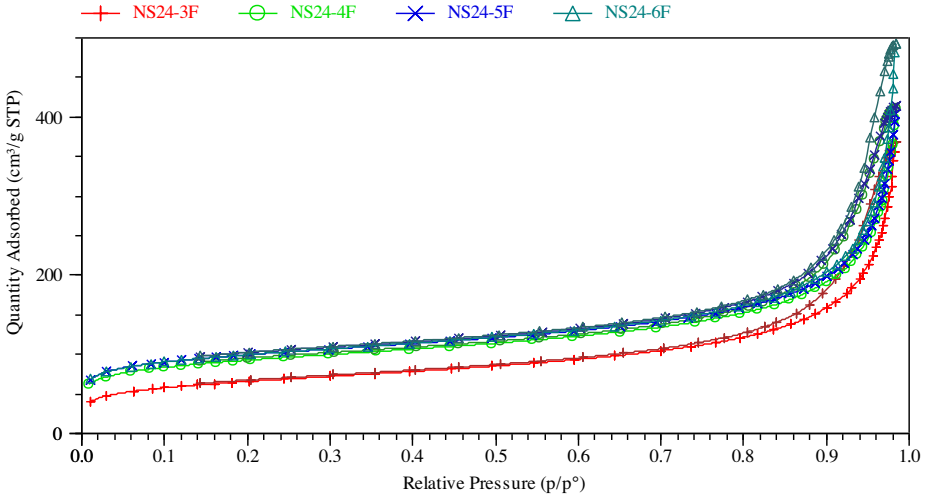

Fig. 5. Adsorption isotherms of the olivine silicas with different number of filtration steps.

conductivity of the filtrate and the total mass of impurities (m_{T_im}) of different silicas. The purity of silica was calculated using:

$$P_{Si}(\%) = m_{SiO_2} + m_{LOI} - m_{SO_3} \quad (2)$$

and was above 99% after the five filtration steps showing the good quality of the silica for the samples using vacuum filtration.

The adsorption isotherm and the t-plot curve for the silica with different washing steps are shown in Figs. 5 and 6, respectively. There was an increase in the SSA with the number of washing steps. During the washing and filtration, the sulfate salts, which are soluble, were removed from the silica. The sulfate salts were adsorbed on the surface area of the silica, and the cleaning could be regarded as an extraction of the salts from the silica [13]. The specific surface area in the micropores for clean silicas (samples with 5 and 6 filtration steps) is 40% of the SSA_{BET}.

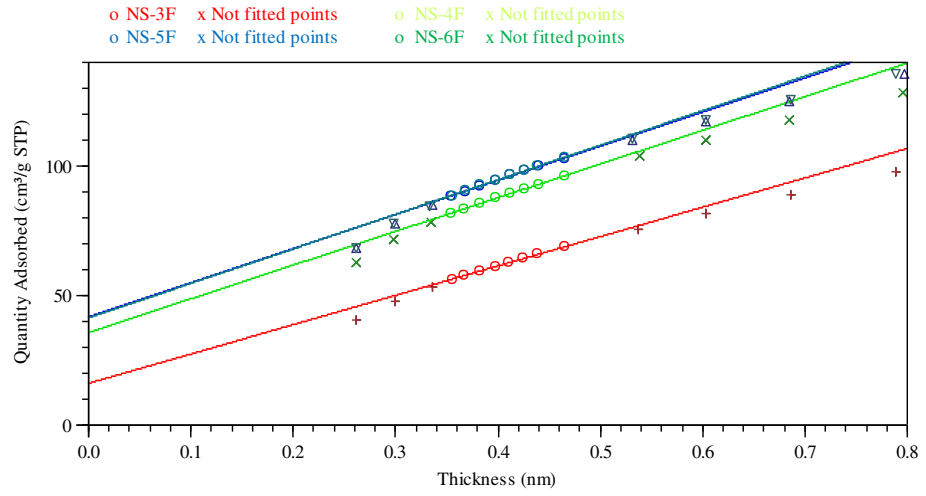

Fig. 6. t-plot curves of the olivine silicas with different number of filtration steps.

Table 4
Estimation of SSA_{BET*} for a sulfate-free silica, volume of impurities, total volume in the micropores and SSA_{MP*}.

Sample	SSA_{BET} (m^2/g)	SSA_{BET*} (m^2/g)	V_{MgSO4} (cm^3/g)	V_{FeSO4} (cm^3/g)	V_{H2SO4} (cm^3/g)	V_{T_im} (cm^3/g)	V_{T_MP} (cm^3/g)	V_{T_im} (%)	SSA_{MP*} (m^2/g)
NS-24–3F	233	250	0.0182	0.0023	0.0096	0.0301	0.0551	54.61	127
NS-24–4F	324	329	0.0053	0.0008	0.0000	0.0061	0.0615	9.91	135
NS-24–5F	346	347	0.0009	0.0000	0.0000	0.0009	0.0652	1.36	149
NS-24–6F	348	348	0.0005	0.0000	0.0000	0.0005	0.0646	0.82	149

Where $MgSO_4$ and $FeSO_4$ are in monohydrate form.
SSA_{BET*} was calculated using Eq. (4) and SSA_{MP*} was calculated using Eq. (5).

Table 5
Experimental conditions of the ripening tests.

Sample	T (°C)	pH	m_{SiO2} (%)	Base	HM (rpm)
RP-1	89	8.4	4.4	NH_4OH	–
RP-2	90	10.0	3.1	NH_4OH	–
RP-3	90	8.3	2.6	NaOH	–
RP-4	90	9.6	3.3	NaOH	–
RP-5[a]	90	10.0	6.6	NaOH	5000
RP-6	RT	9.0	3.1	NaOH	1200
RP-7	RT	9.0	3.1	NaOH	5000
RP-8	RT	9.0	3.0	NaOH	7500
RP-9	RT	4.6	3.1	–	5000
RP-10	RT	7.1	3.1	NaOH	5000
RP-11	RT	11.0	3.0	NaOH	5000

RT refers to room temperature and HM to high shear mixer.
[a] In RP-5 the high shear mixer was used for 10 min in order to break the silica lumps faster.

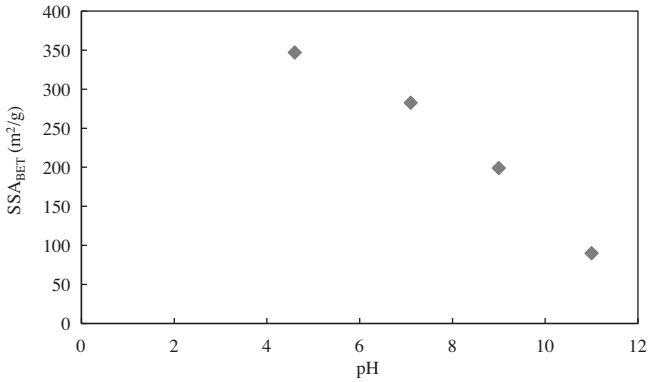

Fig. 7. Reduction of the SSA_{BET} after the Ostwald Ripening treatment using the high shear mixer.

In order to investigate the influence of the sulfate salts on the SSA of silica, two hypotheses are proposed: (1) the only influence of the sulfates on the SSA_{BET} would be their mass, not having any direct effect in the SSA_{BET}. In that case, an SSA_{BET} of the sulfate-free silica (i.e., SSA_{BET*}) can be calculated taking into account that the impurity mass does not contribute to the SSA_{BET}:

$$SSA_{BET*} = \frac{SSA_{BET}}{(1 - m_{T\_im})} \quad (3)$$

(2) The sulfates are located in the micropores partly blocking them. Thus, an SSA_{MP*} could be estimated using the following formula:

$$SSA_{MP*} = \frac{SSA_{MP}}{1 - (V_{T\_im}(\%))/100} \quad (4)$$

where V_{T_im} (%) is the ratio between the total volume of impurities and the total volume in the micropores (V_{T_MP}). Table 4 presents the following values: (a) SSA_{BET*}; (b) the volume of the impurities in the silica using the densities of magnesium and iron sulfate monohydrate (2.45 and 1.9 cm^3/g, respectively) as well as sulfuric acid (1.84 cm^3/g); (c) the total volume in the micropores (V_{T_MP}, see Eq. (6)), with consideration that sulfates are only found in those

Table 6
Surface area, surface area reduction and particle size of the ripened olivine nano-silica.

Sample	Time (h)	SSA_{BET} (m^2/g)	SSA_{MP} (m^2/g)	Red. SSA_{MP} (%)	SSA_E (m^2/g)	Red. SSA_E (%)	d_{p_A} (nm)	d_{p_D} (nm)	d_{BET} (nm)
RM	–	341	102	–	239	–	17	16	8
RP-1	6.0	140	20	80	120	50	20	19	19
RP-1	22.0	124	19	81	105	56	17	16	22
RP-2	3.0	150	22	78	128	47	20	19	18
RP-2	6.0	135	18	82	117	51	19	19	20
RP-3	1.5	181	25	75	156	35	21	20	15
RP-3	6.0	133	18	82	115	52	23	22	20
RP-4	6.0	133	19	81	114	53	18	17	21
RP-5	0.2	159	19	82	140	41	22	20	17
RP-5	6.0	139	19	81	120	50	20	19	20
RP-6	0.2	209	29	71	180	25	20	20	13
RP-6	1.0	197	27	73	170	29	21	20	14
RP-7	0.2	200	28	72	172	28	21	20	14
RP-7	1.0	199	26	74	173	28	22	21	14
RP-8	0.2	203	28	72	174	27	22	20	13
RP-8	1.0	191	26	74	165	31	23	22	14
RP-9	1.0	347	105	–	242	–	17	17	8
RP-10	1.0	283	70	31	212	11	19	19	10
RP-11	0.2	141	16	84	124	48	25	23	19
RP-11	1.0	90	12	89	79	67	28	26	30
RP-11[1]	2.0	101	12	88	89	63	27	24	27

RM refers to the Raw material used (supplied by Geochem).
[1] In sample RP-11 an ultrasound bath was used for 1 h.

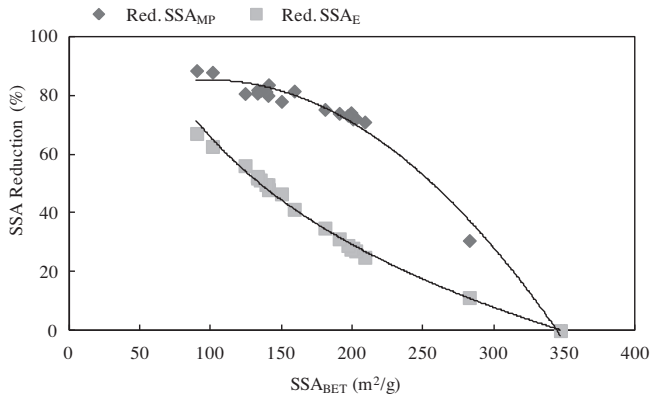

Fig. 8. Reduction of the SSA_{MP} and SSA_E after the Ostwald Ripening treatment using the high shear mixer.

Table 7
d_{10}, d_{50} and d_{90} of the ripened olivine nano-silica dispersion.

Sample	Time	d_{10} (μm)	d_{50} (μm)	d_{90} (μm)
RP-6	10	6.9	16.9	36.0
RP-6	60	6.8	17.5	43.2
RP-7	10	6.3	15.0	31.6
RP-7	60	6.1	13.0	25.0
RP-8	10	5.7	13.8	32.7
RP-8	60	4.9	10.9	24.6
RP-9	60	6.0	14.1	31.5
RP-10	60	6.7	15.7	35.9
RP-11	10	6.54	14.5	29.2
RP-11	60	6.04	14.1	29.7
RP-11[a]	60	4.758	9.8	19.0

[a] In sample RP-11 an ultrasound bath was used for 1 h.

locations; (d) the ratio of the impurity volume regarding this total volume; and (e) the estimated $SSA_{MP}*$.

$$V_{T\_MP} = V_{MP} + V_{T\_im} \quad (5)$$

In the case that the only influence of the sulfates to the SSA_{BET} would be their mass, the $SSA_{BET}*$ should be constant for all the samples; however, $SSA_{BET}*$ increases from 250 to 348 m^2/g. In the case that hypothesis two is accurate, the $SSA_{BET}*$ should be constant for all the samples. Although $SSA_{MP}*$ increases from 127 to 144 m^2/g, the increase is much lower than in hypothesis 1. Hypothesis 2 is also in agreement with the fact that between consecutive filtration steps, particularly between filtration steps 3 and 4, the SSA_{MP} had a higher increase (110%) than the SSA_E (15%).

The purity content of sample NS-HP is lower than sample NS-6F (see Table 3) even though the conductivity levels are similar. This is due to the formation of preferential paths during the filtration of NS-HP making the washing inefficient. Another remarkable fact of sample NS-HP is that in spite of the low purity content, this sample presents a high SSA. This might be due to the compression effect on the bulk structure of the silica and would be in agreement with what Madeline [14] stated about the influence of pressure on the voids of a nanoparticle cake. This idea is also supported by the highest volume of the pores (V_{P_A}) for sample NS-HP. Thus, the fact that the specific surface area does not decrease but increases means that the filtration pressure was high enough to compress the pores of the material, but not high enough to collapse them. If the filtration pressure had been higher, the pores would have collapsed, resulting in a drastic drop of the SSA_{MP} and SSA_{BET}. Therefore, it can be stated that the filtration pressure is a key parameter influencing the specific surface area.

3.2. Ostwald ripening

The experimental conditions of the ripening tests are shown in Table 5 giving the average values of the reactor temperature, the pH, the silica mass percentage and the base used. Table 6 lists the specific surface areas, the specific surface area reductions after the ripening treatment, and the primary particle size (calculated using Eq. (2)) of nano-silica for the raw material used and the treated samples.

The parameters of the ripening experiments were the type of solution, the pH, the silica percentage, the temperature, the reaction time, and the type and speed of mixer. As can be seen in Table 6, the type of solution and the silica percentage do not affect the final SSA_{BET}. In the first three experiments, it was noticed that the silica lumps did not disappear earlier than three hours, but after 10 min with the high shear mixer, the lumps were gone. The speed of the high shear mixer does not affect the final surface area (see RP-7, RP-8 and RP-9). Therefore, it can be stated that the high shear mixer cannot modify the final result of the SSA_{BET} during the Ostwald ripening, but it speeds up the ripening process. The pH and the temperature are the most important factors influencing the final properties of the silica due to the enhancement of solubility.

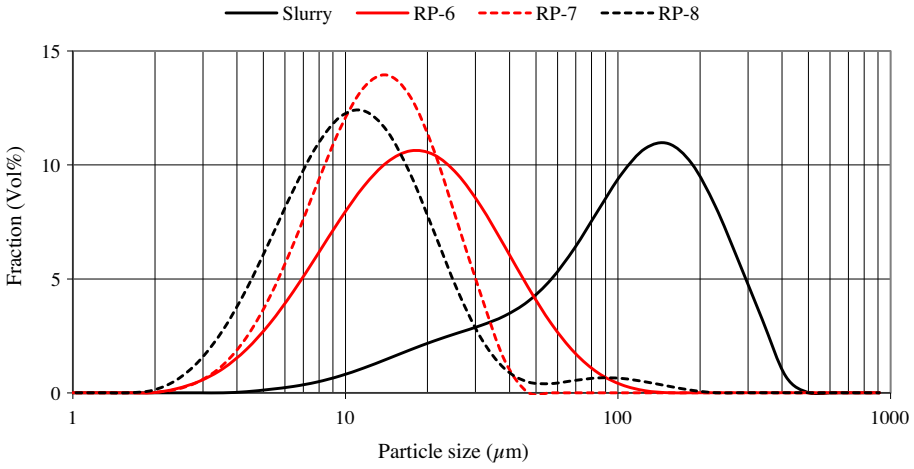

Fig. 9. Particle size distributions of olivine nano-silica dispersions after the Ostwald ripening treatment. Where Slurry refers to a nano-silica slurry produced by the dissolution of olivine [15].

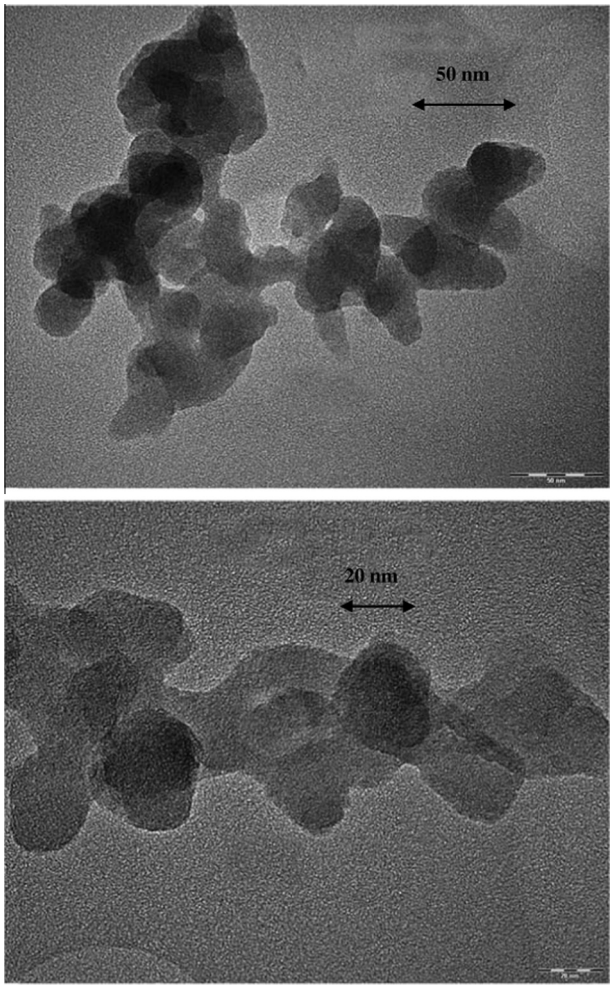

Fig. 10. Transmission electron microscope photographs (250 kx and 430 kx, respectively) of olivine nano-silica after the Ostwald ripening treatment.

The influence of the temperature can be seen comparing experiments RP-3 and RP-4 (pH 8.3 and 9.6 and 90 °C), where the SSA_{BET} decreased up to 133 m^2/g, to experiment RP-6 (pH 9 and 20 °C), where the SSA_{BET} decreased only up to 197 m^2/g. The influence of the pH is illustrated in Fig. 7, where the SSA_{BET} of the ripened samples at room temperature decreases with the pH (90 m^2/g at pH = 11). Fig. 8 shows the variation in the reduction of the SSA_{MP} and SSA_E during the Ostwald ripening. As can be seen from the slopes of the curves, the decrease of the SSA_{MP} is greater than the decrease for SSA_E involving samples with a small reduction of SSA_{BET}. For Sample RP-11, 89% of the micropore area is reduced producing a material with low porosity.

In addition to the specific surface area results, particle size distribution (PSD) analyses were carried out as well (see Table 7 and Fig. 9) for the samples where high shear mixer was used and for the slurry of nano-silica produced by the dissolution of olivine [15]. The PSDs of the ripened dispersions are considerably lower than the PSD of the olivine nano-silica slurry. The d_{50} particle size of the ripened samples were in the range of 13 to 18 μm, and it decreased up to 9 μm in experiment RP-11, where the sample was treated with ultrasounds for 60 min.

TEM photographs of RP-1 are shown in Fig. 10. Agglomerates are still present, and the surface of the silica particles seems to be more rounded than in samples without ripening.

Although the Ostwald ripening treatment of the olivine nano-silica was successful in tailoring the SSA and partly reducing the particle size of the agglomerate, this treatment was not able to break the agglomerates into the primary particles of the olivine nano-silica, not even when the high shear mixer was used.

4. Discussion

In the previous section, the results of the ripening of olivine nano-silica are presented and show a drastic decline of the specific surface area as well as a minor decrease in terms of particle size distribution. In addition, TEM photographs also revealed that the silica particles are more rounded. These changes are due to the Ostwald ripening, where the solubility equilibrium is shifted, and they can be explained by the following hypothesis. The smallest individual silica particles (in the case that individual particles are present in the dispersion) are dissolved into the medium when the solubility is increased by raising the pH or the temperature. Then, part of the soluble silica condensates at the points of lower solubility, which are the connection points between primary particles in the agglomerates. When the individual particles have been removed from the dispersion, and the equilibrium is not yet reached, the external parts of the agglomerates dissolve to condensate afterwards at the connection point between particles. This process continues until the equilibrium is reached and there are no silica particles with different solubilities.

This proposed hypothesis can explain why the agglomerates are still present after the ripening experiments; the decrease of the SSA_{MP} is greater than the SSA_E for samples with a small reduction of SSA_{BET}, and the silica particles seem more rounded (see Fig. 10). The reasons why the agglomerates are still present after the ripening are because neither the high shear mixer can break them into individual particles nor can they be dissolved during the ripening. In fact, the agglomerates could be even stronger since soluble particles condense on the junction between particles strengthening the union. The SSA_{MP} is reduced more than the SSA_E for samples with a small reduction of SSA_{BET} because the soluble silica first condenses in these locations. As the ripening progresses, the reduction of SSA_{MP} gets slower and the reduction of SSA_E speeds up, mainly because the most accessible SSA_{MP} has already been filled with silica.

The solubility of silica cannot be increased much further than pH 11; therefore, the SSA_{BET} cannot be further reduced by this method. An alternative method to further reduce the SSA_{BET} would be to add active silica to the solution. This method is known as the building-up process [6,16,17] and is based on a continuous ripening of nano-silica due to continuous addition of active or reactive

Table 8
The number of moles and masses of sulfur, magnesium and iron of different olivine nano-silicas.

Sample	n_S (mol/g)	n_{Mg} (mol/g)	n_{Fe} (mol/g)	n_{Mg}^* (mol/g)	m_{MgSO4} (%)	m_{FeSO4} (%)	m_{H2SO4} (%)	m_{T_im} (%)
NS-24–3F	5.277E-04	3.214E-04	2.543E-05	3.214E-04	4.4478	0.4321	1.7737	6.6536
NS-24–4F	1.027E-04	9.402E-05	8.743E-06	9.402E-05	1.3010	0.1015	0.0000	1.4013
NS-24–5F	1.563E-05	5.222E-05	6.276E-06	1.563E-05	0.2163	0.0000	0.0000	0.2163
NS-24–6F	9.349E-06	5.453E-05	5.005E-06	9.349E-06	0.1294	0.0000	0.0000	0.1294

Where $MgSO_4$ and $FeSO_4$ are in monohydrate form.

silica. Using this method it is possible to further grow the nano-silica particles, but it has the inconvenience that the agglomerates cannot be broken since the active silica will deposit on them.

5. Conclusions

The process conditions of the olivine nano-silica production have a strong influence on the final specific surface area of this material. Thus, modifying the process conditions, nano-silicas with different specific surface areas can be synthesized. In addition, treatment of the olivine nano-silica by the Ostwald ripening can be a useful method to tailor the specific surface area between 100 and 400 m^2/g.

The process conditions and the ripening process influence the properties of nano-silica in different ways: (1) The cleaner the nano-silica is, the higher the specific surface area is, reaching values between 300 and 400 m^2/g for olivine silicas with low content of salts or silica purities above 99%. The sulfate salts are located in the pores of the silica agglomerates blocking them and drastically reducing the SSA_{MP}. (2) The higher the filtration pressure is, the higher the surface area will be. This is due to a reduction of the pore volume. However, if the pressure is too high, the pores of the material collapse reducing the SSA drastically. (3) The ripening process diminishes the specific surface of nano-silica by three-quarters and could be further reduced if the material would be treated gradually using the building-up process. In addition, this treatment almost completely removes the microporous surface area of the samples.

The results shown here demonstrate that olivine nano-silica can be tailored in the range of 90–400 m^2/g by the ripening treatment in an alkaline solution between pH 8 and 11 at room temperature and by using high shear mixers. Therefore, tailored olivine nano-silica can be produced for different types of applications, with the environmental and economic benefits that the use of this new nano-silica represents regarding the existing commercial products.

Acknowledgements

The authors wish to express their appreciations to P. H. Cappon and J. Nokes for their fruitful discussions and assistance. They furthermore express their gratitude to EU FP7 project ProMine: Nanoparticle products from new mineral resources in Europe (Grant agreement No. 228559). The authors also wish to express their gratitude to the following sponsors of the Building Materials research group at TU Eindhoven: Bouwdienst Rijkswaterstaat, Graniet-Import Benelux, Kijlstra Betonmortel, Struyk Verwo, Attero, Enci, Provincie Overijssel, Rijkswaterstaat Directie Zeeland, A&G Maasvlakte, BTE, Alvon Bouwsystemen, V.d. Bosch Beton, Selor, Twee "R" Recycling, GMB, Schenk Concrete Consultancy, Intron, Geochem Research, Icopal, BN International, APP All Remove, Consensor, Eltomation, Knauf Gips, Hess ACC Systems and Kronos.

Appendix A. m_{T_im} calculation

Table 8 presents the number of moles and masses of sulfur, magnesium and iron, where the magnesium and iron salts are in a monohydrate form at 190 °C [18] (temperature at which the gas physisorption analyses were conducted). In addition, the total mass of impurities is also presented in this table. It is noteworthy that the number of moles of magnesium is higher than the moles of sulfur for samples with low sulfur content, e.g., NS-5F, NS-6F. This is likely due to the different analysis techniques used for determination of oxides and sulfur. For these special cases we calculated the number of moles of magnesium based on the sulfur content ($n^*_{MG} = n_s$) and neglected the value of iron.

References

[1] M.J. Pitkethly, Mater. Today 7 (2004) 20–29.
[2] Cientifica, Half Way to Trillion Dollar Market? A critical Review of the Diffusion of Nanotechnologies, 2007.
[3] Freedonia, World Specialty Silicas, 2010.
[4] A. Lazaro, H.J.H. Brouwers, G. Quercia Bianchi, J.W. Geus, Chem. Eng. J. 211–212 (2012) 112–121.
[5] G. Cao, Nanostructures & Nanomaterials: Synthesis, Properties & Applications, Imperial College Pr., 2004.
[6] R.K. Iler, The Chemistry of Silica: Solubility, Polymerization, Colloid and Surface Properties, and Biochemistry, John Wiley and Sons, 1979.
[7] ISO 9277:2010, Determination of the specific surface area of solids by gas adsorption – BET method, 2010.
[8] S. Brunauer, P.H. Emmett, E. Teller, J. Am. Chem. Soc. (1938) 309–319.
[9] J.H. de Boer, B.G. Linsen, T. Osinga, J. Catal. 4 (1965) 643–648.
[10] W.H. Harkins, G. Jura, J. Am. Chem. Soc. (1944) 1366–1373.
[11] E.P. Barrett, L.G. Joyner, P.P. Halenda, J. Am. Chem. Soc. (1951) 373–380.
[12] Micromeritics, Tristar II 3020 – Operator's manual V1.03, 2009.
[13] D.J. Lieftink, The preparation and characterization of silica from acid treatment of olivine, PhD Thesis, Utrecht University, 1997.
[14] J.B. Madeline, M. Meireles, C. Bourgerette, R. Botet, R. Schweins, B. Cabane, Langmuir 23 (2007) 1645–1658.
[15] A. Lazaro, G. Quercia, H.J.H. Brouwers, Production and Application of a New Type of Nano-Silica in Concrete, International Conference on Building Materials, Ibausil, 2012.
[16] M. Mindick, P.H. Vossos, Large particle silica sols and method of, production, [US3538015], 1970.
[17] D.L. MacDonald, Method of producing silica sols with controllable broad size distribution and minimum particle size, [US2009/0018219A1], 2009.
[18] H. Tagawa, Thermochim. Acta 80 (1984) 23–33.
[19] ECETOC, Synthetic Amorphous Silica (CAS No. 7631-86-9), Joint Assessment of Commodity Chemicals (JACC) Report No. 51, Brussels, 2006.